

Cold atmospheric plasma modulates endothelial nitric oxide synthase signalling and enhances burn wound neovascularisation

Constance Duchesne^{1,2}, Sébastien Banzet¹ , Jean-Jacques Lataillade^{1†}, Antoine Rousseau^{2†} and Nadira Frescaline^{1,2*} 

¹ Institut de Recherche Biomédicale des Armées, Centre de Transfusion Sanguine des Armées, Clamart, France

² Laboratoire de Physique des Plasmas, École Polytechnique, UPMC, Université Paris Sud 11, Palaiseau, France

*Correspondence to: N Frescaline, Institut de Recherche Biomédicale des Armées, INSERM UMRS-MD 1197, Centre de Transfusion Sanguine des Armées, 92141 Clamart, France. E-mail: nadira.frescaline@pp.polytechnique.fr

†These authors are senior investigators.

Abstract

Treatment with cold atmospheric plasma (CAP) has been reported to promote wound healing in animals. However, how this process is mediated remains unclear. In this study we examined the mechanisms which underlie the improved wound healing effects of CAP and the roles of associated reactive oxygen and nitrogen species (RONS), which are generated by plasma. By using *in vitro* models which mimicked various steps of angiogenesis, we demonstrated that CAP triggered the production of nitric oxide (NO), and enhanced cell migration and the assembly of endothelial cells into vessel-like structures. These are both hallmarks of the proliferative phase of wound healing. Using a mouse model of a third-degree burn wound, we went on to show that CAP treatment was associated with enhanced angiogenesis, characterised by accelerated *in vivo* wound healing and increased cellular proliferation. Here, CAP significantly increased the *in vivo* production of endothelial NO synthase (eNOS), an enzyme that catalyses NO synthesis in endothelial cells, and significantly increased the expression of pro-angiogenic PDGFR β and CD31 markers in mouse wounds. Mechanistically, we showed that CAP induced eNOS phosphorylation and activation, thereby increasing the levels of endogenous NO in endothelial cells. Increased NO generation facilitated by CAP further stimulated important pro-angiogenic VEGFA/VEGFR2 signalling *in vitro*. This proof-of-concept study may guide future efforts aimed at addressing the use of physical plasma and its therapeutic applications in a variety of pathological scenarios.

© 2019 Pathological Society of Great Britain and Ireland. Published by John Wiley & Sons, Ltd.

Keywords: full-thickness burn wound; cold atmospheric plasma; NO; RONS; VEGF; wound healing; eNOS; angiogenesis; skin graft

Received 1 April 2019; Revised 12 June 2019; Accepted 27 June 2019

No conflicts of interest were declared.

Introduction

Severe burn injuries pose a significant challenge for healthcare providers across the globe. This is in large part due to a multitude of associated health complications such as wound infection and sepsis [1]. Furthermore, the process of burn wound healing is complex and in order to be successful, requires robust and coordinated cellular migration, proliferation, and neovascularisation responses [2,3]. Allogeneic skin graft transplantation remains the gold standard treatment for severe burns, particularly those which cover a high percentage of a patient's body [4]. However, this approach is often undermined by the ability of skin grafts to successfully integrate into a recipient site [3]. Engraftment success is dependent on wound angiogenesis, which restores damaged vasculature at the wound site and establishes vascular anastomoses between the recipient bed and the graft [5]. Wound angiogenesis is regulated by a combination

of endogenous growth factors, inhibitors, and mediators of vascular response [6,7]. Nitric oxide (NO) is one such endogenous signalling molecule which promotes wound healing by stimulating the angiogenic cascade [8,9]. In endothelial cells, NO is produced by endothelial NO synthase (eNOS), which catalyses the oxidation of L-arginine into citrulline and NO [10]. As a result, eNOS knockout and arginine-deficient animals are associated with delayed wound healing [10,11], whereas exogenous addition of NO improves tissue repair in various model systems [12–14], including burn wounds [15–17]. Given its beneficial effect on tissue repair, development of new and improved NO-based strategies is justified.

In this study, cold atmospheric plasma (CAP) was used to stimulate endogenous NO production. CAP is made up of weakly ionised gas [18] with an ionisation degree typically $\leq 0.01\%$. The electric discharge used to generate CAP facilitates the production of energetic electrons which excite, dissociate, and ionise gas molecules [19]. CAP devices have been tested in pilot

clinical studies which involved acute [19] and chronic wounds [20]. Although previous studies demonstrated therapeutic efficacy and simplicity of administration [18,21], the mechanisms by which CAP triggers biological responses are poorly understood. In open air, CAP has been shown to produce reactive oxygen and nitrogen species (RONS) [22]. Given that neovascularisation is important for tissue repair [2] and other pathological conditions [7], we hypothesised that CAP-generated RONS, such as NO, enhance angiogenesis via modulation of eNOS/NO signalling. The aim of this study was two-fold: to identify mechanisms that may explain enhanced microvessel assembly and angiogenic growth factor release in endothelial cells treated with CAP, and to investigate the effect of CAP on tissue repair and wound angiogenesis in a mouse model of a third-degree burn reconstructed with a skin graft, which has never been described previously.

Materials and methods

Mouse model of third-degree burn wound reconstructed with full-thickness skin graft

All experiments were approved by the relevant Animal Ethics Committee (No 12216-2017111616517670v2). BALB/c mice were anaesthetised using an intraperitoneal injection of xylazine (10 mg/kg) and ketamine (100 mg/kg). Buprenorphine (0.05 µg/g) was administered subcutaneously as analgesia to control post-procedural pain. The animals were positioned prone on a flat table and thermal burns were created by applying a circular brass block (10 mm in diameter), preheated to 80°C. A digital manometer with pressure indicator was used to ensure constant pressure between the brass block and mouse skin. A third-degree burn (80°C for 20 s) was created on the dorsum of the mouse. Necrotic tissue was excised 24 h after the injury. In all instances, skin graft refers to the use of a full-thickness skin graft fashioned from the tail of a donor mouse. Skin grafts (15 mm) were laid over the excised burn wounds. The grafts were then secured with a surgical adhesive (Leukosan; BSN medical, Quickbornstraße, Hamburg, Germany). All wounds were covered with Adaptic (Systagenix, North Yorkshire, UK) and Micropore™ Surgical Tape (3M, Cergy-Pontoise, France). The treatment groups included (i) unionised helium gas (placebo control, 30 s), (ii) CAP (30 s, 24 kV), (iii) topical application of glyceryl trinitrate ointment (NO donor; 1.5 mg; Kyowa Kirin Pharma, Neuilly-sur-Seine, France), (iv) transdermal nitroglycerine patch (NO donor; 1.25 mg; Lavipharm Laboratories, Alloga, France), and (v) intraperitoneal injection of NO synthase inhibitor N^G-nitro-L-arginine methyl ester (L-NAME; 20 mg/kg; Sigma-Aldrich, St Quentin Fallavier, France). In all instances, grafted wounds were treated every 48 h and harvested at day 7 post-burn injury. Further details of mouse studies are available in the supplementary material, Supplementary materials and methods.

Cold atmospheric plasma treatment

CAP was generated using a plasma jet. The plasma source was manufactured from polylactic polymer using a 3D printer. The plasma source consisted of a 50 Hz high AC voltage electrode and a capillary (length 60 mm; inner diameter 3 mm). Helium gas [0.5 standard L/min (SLM)] was passed through the capillary bore. CAP was produced in the vicinity of the high voltage electrode and propagated from the source to the target in the form of a single channel plasma jet. RONS were formed at the output of the capillary when the plasma interacted with the ambient air. CAP had a characteristic sound and a blue light in the dark. Voltage was set to 24 kV for *in vivo* and 32 kV for *in vitro* and *ex vivo* experiments. Electrical signals were monitored and collected with an RTE1024 oscilloscope (Rohde & Schwarz, Columbia, MD, USA) using the Lissajou method. Mouse skin temperature was monitored during the CAP treatment using an infrared thermal imaging camera (Testo Ltd, Alton, Hampshire, UK). CAP had no effect on mouse skin temperature. The electrode was placed 5–10 mm above the skin.

Matrigel plug assay

Two plugs (500 µl each) containing Matrigel (Corning, Tewksbury, MA, USA), rmFGF (100 ng/ml), rmVEGF (100 ng/ml), and heparin (25 U) were injected subcutaneously into the latero-dorsal region of the mouse abdomen. Implanted plugs were treated with either helium (control) or transcutaneous CAP every 48 h. Microscopic assessment of vascular burden was performed as described previously [23]. The plugs were homogenised and supernatants were mixed with Drabkin's reagent (Sigma-Aldrich) to determine the concentration of haemoglobin (as an indication of vascularity). A fluorescent probe specific to vascular endothelial cells (TLectinSense™ 680; PerkinElmer, Boston, MA, USA) was administered intravenously, and live imaging was performed 6 and 24 h after injection. Whole-body imaging and analysis were performed using IVIS Spectrum Imaging, and Living Image 4.5.5 (PerkinElmer).

Histology, immunohistochemistry, and image analysis

Histological sections (4 µm thickness) were prepared from formalin-fixed and paraffin-embedded tissue and stained with H&E or subjected to immunohistochemistry using a Leica Bond III (Leica Biosystems, Nanterre, France). Primary antibodies (detailed in the supplementary material, Supplementary materials and methods) were applied and incubated for 1 h. Detection was performed by species-specific horseradish peroxidase (HRP) or alkaline phosphatase (AP)-conjugated secondary antibodies. Sections were reacted with one of two substrates: (i) for HRP, 3,3'-diaminobenzidine (DAB) with Bond enhancer (AR9432; Leica Biosystems, Wetzlar, Germany), which produced a brown to

black colour; or (ii) for AP, Bond Polymer Refine Red (DS9390; Leica Biosystems), which yielded a bright red colour. For verification of staining, non-specific binding was determined by omitting primary or secondary antibodies. All control sections showed negligible staining. Stained sections were scanned using a Lamina instrument (PerkinElmer, Waltham, MA, USA) and analysed with the CaseViewer digital microscope application (3DHISTECH, Budapest, Hungary) and ImageJ software. The histological dermal wound length was determined by measuring the distance between the dermal wound margins. Quantification of immunohistochemical staining was performed using a colour deconvolution image analysis algorithm as described previously [24].

Statistical analysis

Statistical analysis was performed using the GraphPad Prism 6.04 software (GraphPad Inc, San Diego, CA, USA). For a two-group comparison, a Student's *t*-test was used, provided that the pre-test for normality (D'Agostino–Pearson normality test) was not rejected at the 0.05 significance level; otherwise, a non-parametric Mann–Whitney *U*-test was used. All data were expressed as mean \pm SEM and *P* values less than 0.05 (*), 0.01 (**), or 0.001 (***) were considered to be statistically significant. The sample size and number of biological replicates are indicated in the figure legends.

Details of the primary cell culture, antibodies and reagents, cell migration and scratch wound assays, cell viability analysis, Matrigel tube formation assays, 3D sprouting angiogenesis assays, aortic ring assays, nitrite/nitrate production and NO detection in HMVECs, immunofluorescence and confocal microscopy, immunohistochemical analysis of *in vivo* wounds, western blotting, and RT-qPCR are given in the supplementary material, Supplementary materials and methods.

Results

CAP enhanced cellular migration and sprouting angiogenesis

Human microvascular endothelial cells (HMVECs) were grown to confluency and challenged with low (2.15 J/cm³) or high (7.78 J/cm³) doses of CAP. Low doses of CAP had no detrimental effect on cellular viability; however, the high dose produced significantly more non-viable cells compared with helium-treated controls, indicating a dose-dependent effect of CAP-induced oxidative stress (supplementary material, Figure S1A,B). Therefore we used low doses of CAP in subsequent experiments. To mimic the cell migration that occurs during wound healing *in vivo*, we performed an *in vitro* scratch assay [25]

to monitor HMVEC motility (supplementary material, Figure S2A). *In vitro* scratch wounds closed significantly faster when treated with low doses of CAP (supplementary material, Figure S2B, *p* < 0.05 versus time-matched controls). To examine this further, we also tested cells using the Radius™ migration assay (supplementary material, Figure S2C). HMVECs were treated with CAP and the cell-free area was measured at 24 h after treatment. Cellular migration was enhanced in CAP-treated HMVECs (supplementary material, Figure S2D, *p* < 0.05 versus time-matched controls).

Having established that CAP enhances cellular migration, it was next hypothesised that CAP may also modulate angiogenesis. A capillary tube formation assay was used to assess whether CAP effects the ability of a network of cells to reorganise into large aggregates and subsequently form capillary tubes and hexagonal loops (Figure 1A). The average loop area was significantly elevated in HMVECs treated with CAP compared with time-matched controls (Figure 1B, *p* < 0.001; CAP versus time-matched controls). In a 3D assay of sprouting angiogenesis, HMVECs were treated with either helium (control), rhVEGF (positive control), or CAP, and assessed for sprout and anastomosis formation (Figure 1C–E). Significantly longer sprout length (Figure 1C, *p* < 0.01 CAP versus time-matched controls) was associated with CAP treatment (Figure 1D,E). In an *ex vivo* assay, mouse aortic rings treated with CAP showed significantly higher numbers of vessel outgrowths (Figure 1F–H, *p* < 0.05 CAP versus time-matched controls). Emerging microvessels were immune-positive for von Willebrand factor (an endothelial cell marker) (Figure 1G).

Increased *in vivo* angiogenesis in response to CAP

Having established that CAP increased sprouting angiogenesis *in vitro*, we next examined its effect on new blood vessel formation *in vivo*. We monitored angiogenesis in a mouse model using a Matrigel plug assay following intravenous injection of TLectinSense™ 680 (an endothelial cell imaging agent). 2D visualisation of plugs implanted in live animals was used to assess the vascular burden (Figure 2A). *In vivo* whole-animal imaging showed that the vascular fluorescent signals generated by CAP-treated plugs were significantly stronger compared with helium-treated controls (Figure 2C; *p* < 0.01 CAP versus control). *Ex vivo* imaging of the Matrigel plugs gave similar results (Figure 2B,C; *p* < 0.001 CAP versus control). Digital images of Matrigel plugs were captured to visualise the formation of vasculature (Figure 2D). Haemoglobin concentration in the supernatants of homogenised Matrigel plugs was higher in CAP-treated samples than in control (Figure 2E; *p* < 0.01 versus control). Matrigel plugs were immunostained for CD31 (endothelial cell marker; green) and TLectinSense™ 680 (fluorescent vascular probe; red) (Figure 2F). H&E-stained sections were assessed for vascular density (Figure 2F). Vessels were categorised as either (i) vessels containing

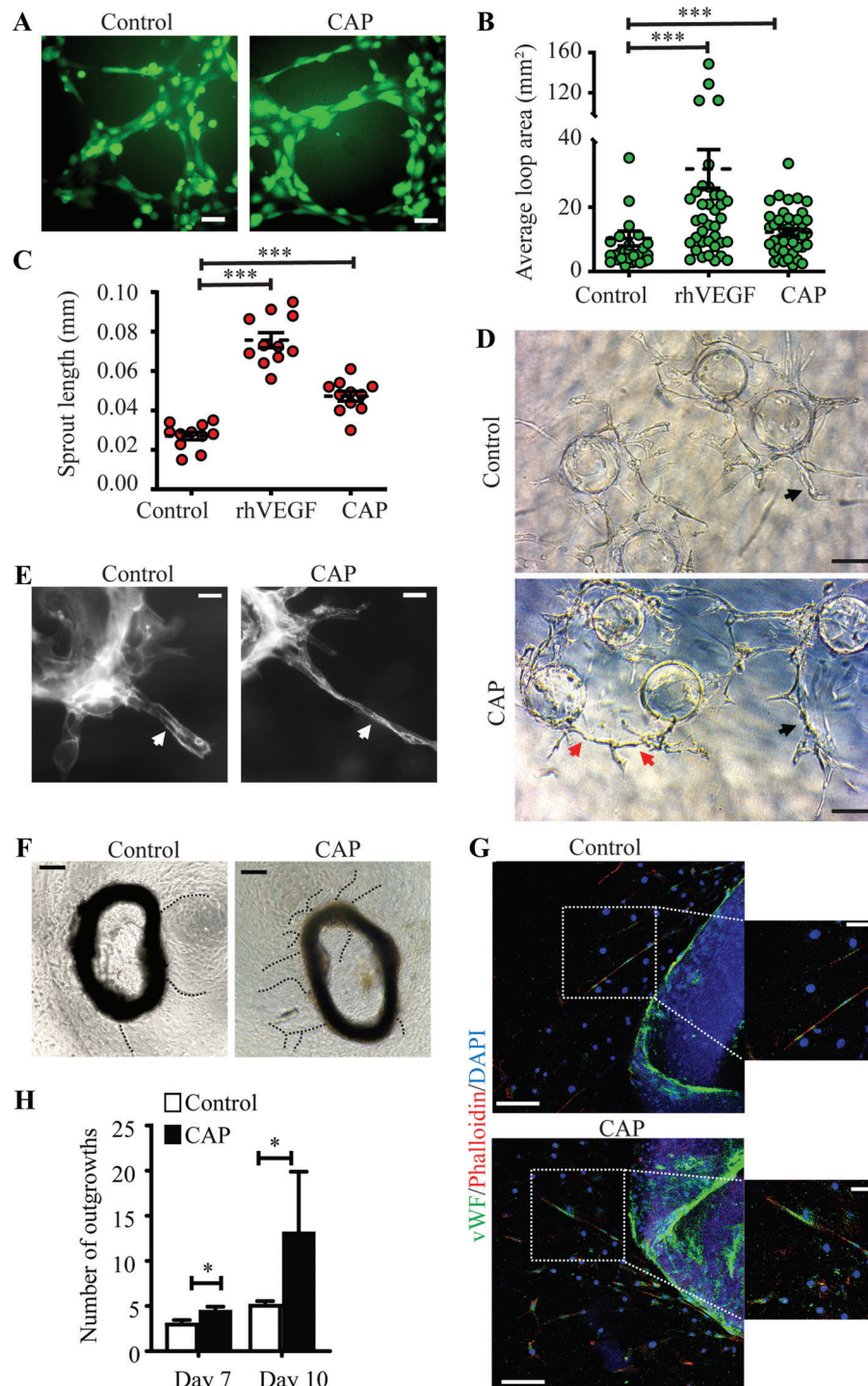


Figure 1. Effect of CAP on sprouting angiogenesis *in vitro* and *ex vivo*. (A) HMVECs were plated onto Matrigel and treated with either helium (control), rhVEGF (positive control) or CAP. Capillary tube formation was monitored for 6 h. Representative images of calcein-stained capillary tubes are shown. Scale bar = 50 μ m. (B) Quantification of the average area of closed capillary loops based on 4 \times images taken at 6 h after treatment with either helium (control), rhVEGF (positive control) or CAP. Mean \pm SEM ($n \geq 20$, *** $p < 0.001$, Mann-Whitney *U*-test). (C) Microcarrier beads were coated with HMVECs, embedded in fibrin matrix, and co-cultured with primary human skin fibroblasts. Coated beads were treated with either helium (control), rhVEGF (positive control), or CAP at days 0, 2, 4, and 6 after embedding in fibrin matrix. Cultures were maintained for 7 days. Graphical representation of vascular sprout length at 7 days post-embedding. The data of the sprout analysis are expressed as the values for repeated conditions in separate wells (average of 20 beads per well). Mean \pm SEM ($n \geq 11$, *** $p < 0.001$, Mann-Whitney *U*-test). (D) Phase-contrast microscopic images showing microcarrier beads with vascular sprouts at 7 days after embedding. Black arrows indicate sprouts; red arrows indicate anastomosis. Scale bar = 50 μ m. (E) Fluorescence microscopy images of fibrin-embedded microbeads stained with phalloidin to highlight the microvessel-like structures (white arrow). Scale bar = 20 μ m. (F) Phase-contrast images of mouse aortic rings embedded in type I collagen showing microvessel outgrowth at day 7 after embedding. Scale bar = 100 μ m. (G) Confocal immunofluorescence images of control and CAP-treated aortic rings. vWF (green) stained endothelial cells (white arrows); phalloidin (red) indicates supporting cells. DAPI-stained nuclei (blue). Scale bar = 20 μ m. Enlarged views of the boxed regions (left panel); scale bar = 5 μ m. (H) Time course of microvessel sprouting of mouse aortic rings treated with helium (control) or CAP. Microvessel sprouts were counted on days 7 and 10 after embedding in type I collagen. Mean \pm SEM ($n = 10$, * $p < 0.05$, Student's *t*-test).

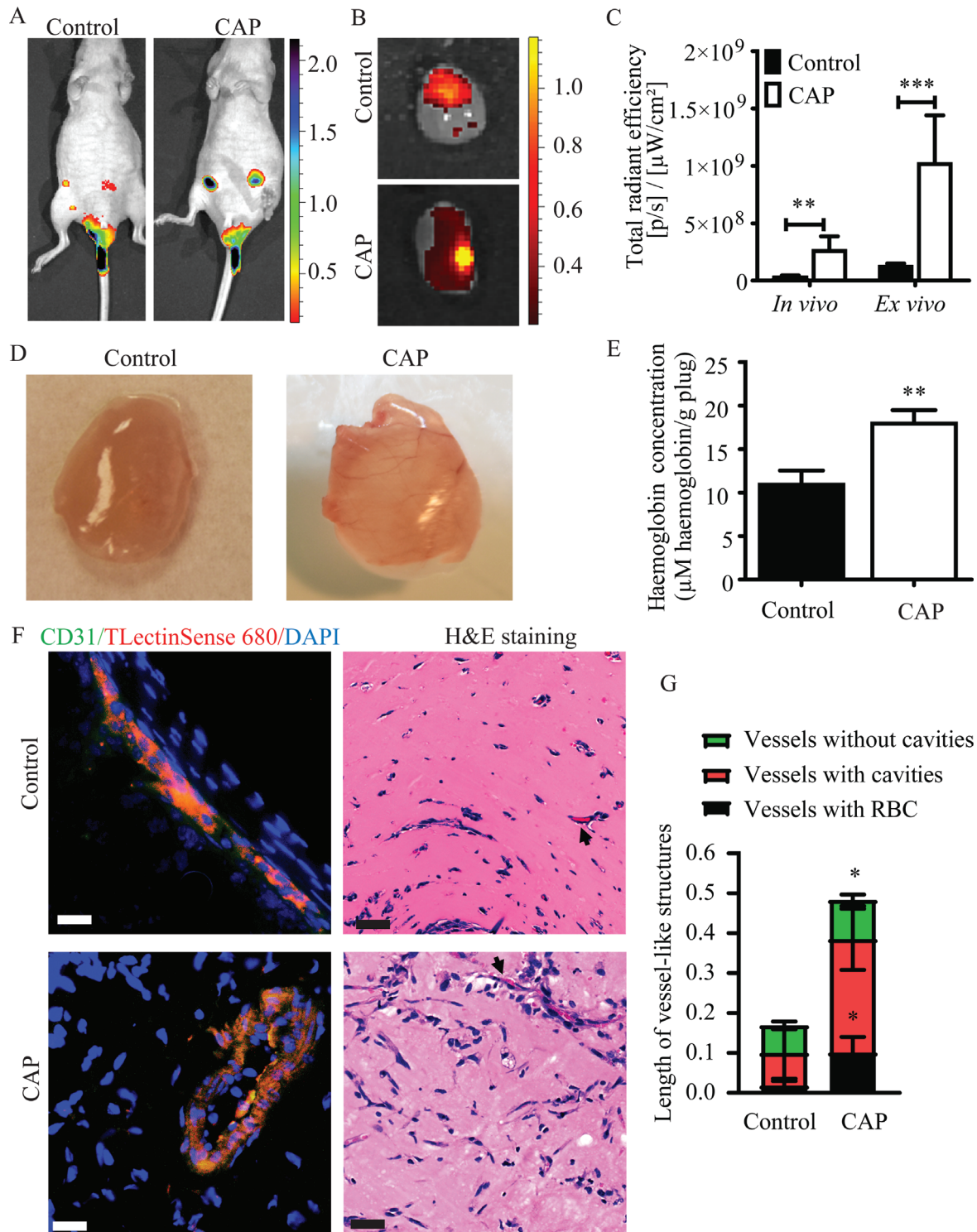


Figure 2. Effect of CAP on *in vivo* angiogenesis. (A) Whole-body imaging at day 9 after subcutaneous implantation of Matrigel plugs. TLectinSense™ 680 (vascular imaging probe) was administered intravenously and live imaging was performed 6 h after injection. Vascular signal of adjacent tissues was excluded for clarity. Autofluorescence before probe injection was taken into account. (B) *Ex vivo* imaging of TLectinSense™ 680 at 6 h after injection. A significantly stronger TLectinSense™ 680 signal was detected in CAP-treated plugs compared with helium-treated controls. (C) Graphical representation of total radiant efficiency based on *in vivo* and *ex vivo* imaging. Matrigel plugs treated with CAP demonstrated significantly higher radiant efficiency than helium-treated controls. Mean \pm SEM ($n = 5$ mice; total number of plugs per condition = 10 with 2 plugs per mouse; *** $p \geq 0.001$; Student's *t*-test). (D) Digital images of Matrigel plugs excised 9 days after implantation. (E) Haemoglobin content of homogenised Matrigel plugs. Haemoglobin concentration was normalised to the weight of the Matrigel plug ($n = 5$, ** $p \geq 0.01$; Student's *t*-test). (F) Dual immunofluorescence images demonstrating CD31⁺ (green) and TLectinSense™ 680⁺ (red) (scale bar = 20 μ m) vessels in snap-frozen Matrigel plugs. H&E staining on paraffin-embedded Matrigel plugs. Scale bar = 50 μ m. Arrowheads indicate vessels containing RBCs. (G) Quantification of new vessel formation in Matrigel plugs by their lengths. Vessels and vessel-like structures were classified as follows: (i) mature blood vessels containing RBCs; (ii) vessels with cavities but without RBCs; and (iii) cells arraying in line but without cavities. The data are the average of eight fields of microscopic view per plug. Mean \pm SEM ($n = 5$, * $p < 0.05$; Student's *t*-test).

erythrocytes, (ii) vessels without erythrocytes, or (iii) vessel-like structures that lacked a lumen. CAP treatment resulted in enhanced formation of two types of vessels, those with and without erythrocytes, yielding a two-fold increase in length when compared with the control (Figure 2G; $p < 0.05$; functional vessels with and without erythrocytes; CAP versus control).

CAP increased the bioavailability of NO in endothelial cells

Given that plasma jets produce RONS, including NO [18], and exogenous NO-delivering platforms improve tissue repair [13,14,26], we next questioned whether CAP was able to trigger endogenous NO production. A cell-permeable NO indicator with nanomolar sensitivity was used to assess intracellular NO by flow cytometry. *S*-Nitroso-*N*-acetylpenicillamine (SNAP, an NO donor) and rhVEGF are positive regulators of NO [27] and were used as positive controls (Figure 3A). Confluent monolayers of HMVECs treated with CAP displayed a four-fold increase in the number of NO-producing cells compared with those treated with helium (control) (Figure 3B; $p < 0.05$; CAP versus control).

Directly measuring NO in liquids is difficult because of its short chemical half-life [28]; we therefore used nitrite (NO_2^-) and nitrate (NO_3^-) as indicators of NO generation. L-NAME is an inhibitor of NO synthase known to block NO production. The concentrations of NO_2^- and NO_3^- were greater in supernatants of CAP-treated HMVECs (Figure 3C; $p < 0.05$; CAP versus control). This effect was blocked by L-NAME, suggesting that CAP treatment stimulated endogenous production of NO in an eNOS-dependent manner (Figure 3C; $p < 0.01$; CAP versus CAP + L-NAME).

Accelerated burn wound healing in response to CAP treatment

Having established that CAP stimulated endogenous NO production *in vitro*, we next compared the effect of CAP with other NO delivery platforms *in vivo*. Exogenous addition of NO donors is known to enhance burn wound healing [15,16]. A mouse model of a third-degree burn treated with an allogenic full-thickness skin graft was used to examine the effect of CAP on burn healing and graft integration. Exposure of skin to 80°C for 20 s consistently produced third-degree burn wounds, which macroscopically appeared as circular wounds with white eschar (Figure 4A). When the eschar and hyperaemic zones were debrided 24 h after injury, the size of the resulting wound was larger than that of the initial burn. Grafted wounds treated with either CAP, topical application of NO donor, or a transdermal application of NO donor showed no signs of transplant rejection. Instead, graft healing was readily observed (Figure 4A). In contrast, wounds treated with L-NAME displayed signs of delayed healing (Figure 4A). Histological dermal wound length was determined by measuring the distance between the dermal margin of

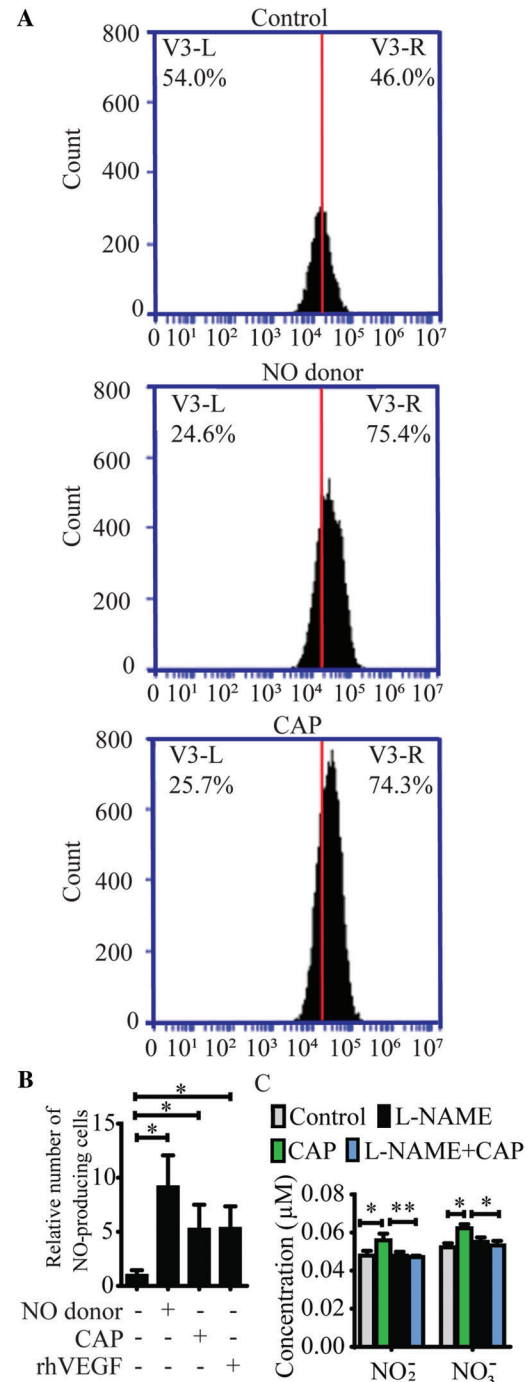


Figure 3. CAP stimulated NO production in endothelial cells. HMVECs were treated with either helium (control), SNAP (NO donor), hrVEGF (100 ng/ml; positive control) or CAP, and incubated for 1 min before harvesting. Intracellular expression of NO was determined by staining HMVECs with DAF-FM (indicator of NO) and analysed by flow cytometry. (A) Representative histograms and (B) graphical representation of fluorometric detection of NO indicate a significantly higher number of NO-producing cells in CAP-treated samples compared with fewer NO-producing cells in helium-treated controls. Representative data from three independent experiments are shown. Mean \pm SEM ($n = 6$, $p < 0.05$, Mann-Whitney *U*-test). (C) Determination of NO via its metabolites (NO_2^- and NO_3^-) was performed using the Griess assay. Sub-confluent monolayers of HMVECs were treated with (i) helium (control), (ii) CAP, or (iii) pre-incubated with NO inhibitor L-NAME (100 μM ; 1 h; negative control) and then treated with CAP. Supernatants were collected 1 min after treatment with CAP. Mean \pm SEM ($n = 5$, $*p < 0.05$; $**p < 0.01$, Mann-Whitney *U*-test).

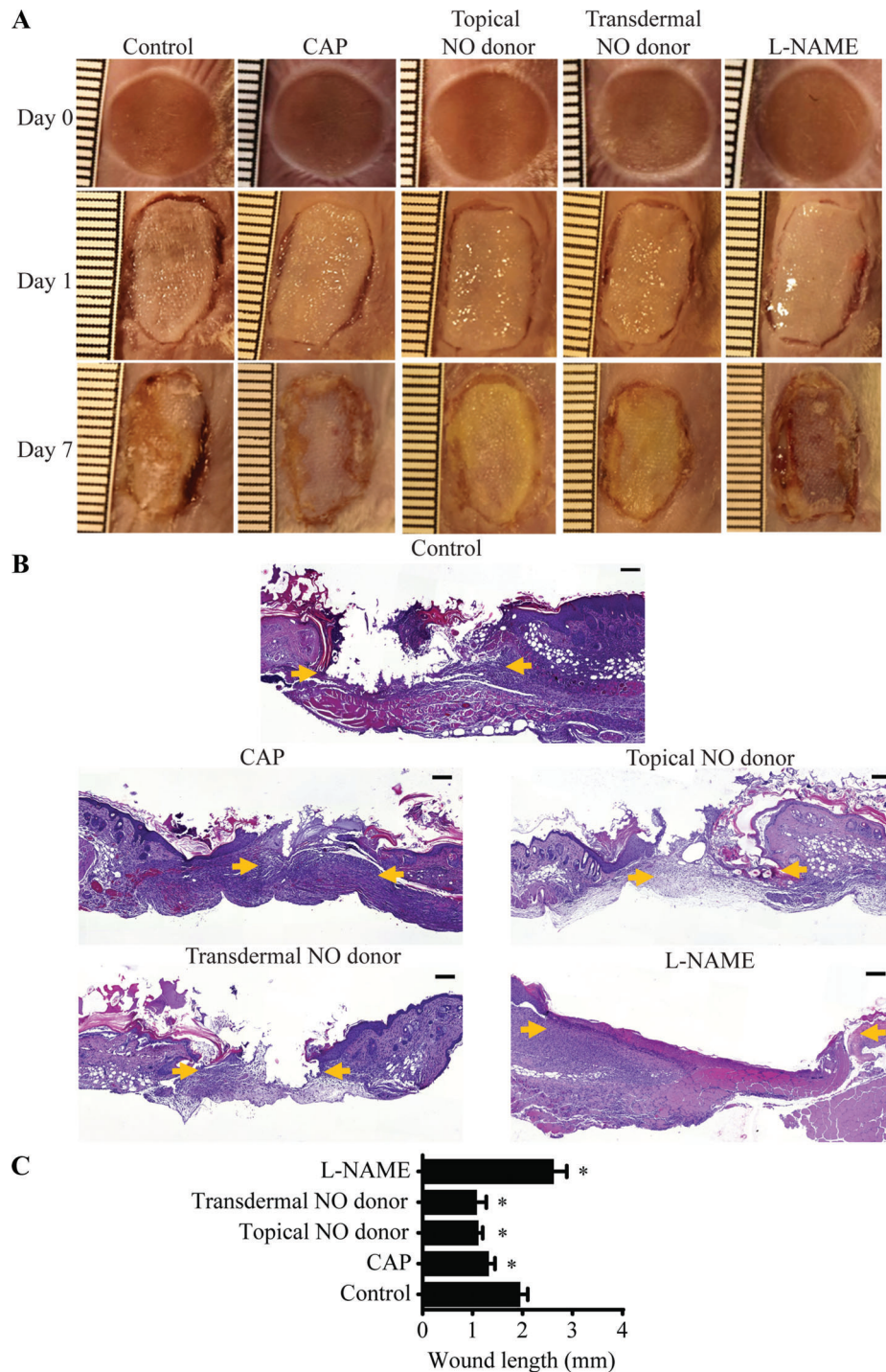


Figure 4. CAP treatment enhanced burn wound healing in mice. To explore the influence of CAP on burn repair, and to determine whether the beneficial effect of CAP was due to its ability to trigger NO production, exogenous NO was delivered to the skin. Burns were induced on the dorsum of each mouse. Burned skin was excised and covered by allogenic skin graft. Wounds were treated with either helium (control), CAP, topical NO donor ointment, or transdermal NO donor patch. NO synthase inhibitor (L-NAME) was administered by intraperitoneal injection. (A) Representative digital images of burn wounds and skin grafts on days 0, 1, and 7. The ruler in the images shows millimetres ($n = 6$). (B) Representative images of H&E-stained sections of wounds 7 days post-burn injury. Orange arrows indicate the wound margins (i.e. wound length). Scale bar = 500 μm . $n = 6$. (C) Graphical representation of wound length. Histological dermal wound length was determined by measuring the distance between the dermal margin of the burn wound and the dermal margin of the skin graft. Mean \pm SEM ($n = 6$, *denotes significance; $p < 0.05$: control versus CAP, topical NO donor, transdermal NO donor, and L-NAME; Student's t -test).

the burn wound and the dermal margin of the skin graft. Histological wound length was significantly shorter in wounds treated with CAP, topical, and transdermal NO donor compared with time-matched helium-treated controls (Figure 4B,C; $p < 0.05$; CAP versus control).

Healing of wounds treated with L-NAME was severely delayed (Figure 4C; $p < 0.05$; L-NAME versus control). To assess the rate of cellular proliferation, wounds and grafts were immunostained with the antibody Ki67 (as a proliferation marker) (supplementary material, Figure

S3A). Treatments with either CAP or NO donors (both topical and transdermal) were associated with increased Ki67 staining (supplementary material, Figure S3B; $p < 0.01$ in CAP and topical NO donor versus control; $p < 0.05$ in transdermal NO donor versus control).

CAP modulated eNOS expression *in vivo* and enhanced burn wound angiogenesis

To assess *in vivo* angiogenesis, burn wounds at day 7 were stained with antibodies to CD31 (an endothelial cell marker) (Figure 5A). CD31 expression was significantly increased in CAP-treated wounds compared with helium control (Figure 5A,C; $p < 0.05$; CAP versus control). Wound angiogenesis is regulated by various growth factors and their receptors, of which VEGFA, PDGFB, and FGF-2 are key players [7]. Although VEGFR2 levels remained unchanged, PDGFR β expression was elevated in response to CAP treatment (Figure 5C; $p < 0.05$; PDGFR β in CAP versus control). To prevent pathologic overgrowth of existing vessels, production of anti-angiogenic molecules including the matrix protein thrombospondin-1 (TSP-1) is required [7]. CAP-treated wounds were associated with lower TSP-1 density compared with controls (Figure 5B,C; $p < 0.01$ in CAP, topical, and transdermal NO versus control).

Given that angiogenesis was enhanced in burn wounds in response to CAP treatment, we then assessed if this observation was, at least in part, due to modulated expression of eNOS – an enzyme responsible for the synthesis of diffusible endothelial NO in the skin [10]. Day 7 wounds treated with CAP or helium were immunostained with an anti-eNOS antibody (Figure 5D). Immunofluorescence analysis of eNOS revealed that wounds treated with CAP contained a higher percentage of eNOS-positive cells compared with controls (Figure 5E; $p < 0.05$; CAP versus control).

CAP activated VEGF receptor and eNOS signalling pathways *in vitro*

To identify the mechanisms that facilitated angiogenesis *in vitro*, we next investigated the effect of CAP on several well-described pro- and anti-angiogenic molecules. RNA and protein extracts were prepared from HMVECs grown to confluence and treated with CAP. A two-fold increase in *VEGFA* mRNA expression was detected in HMVECs treated with CAP compared with controls (Figure 6A; $p < 0.05$; CAP versus control), although mRNA levels of *FGF2* (a gene that codes for fibroblast growth factor-2, a pro-angiogenic protein expressed by endothelial cells [29]) and *COL18A1* (encoding sequences found in endostatin, an anti-angiogenic protein [30]) remained unchanged. A two-and-a-half-fold increase in *PDGFB* mRNA expression was associated with CAP treatment (Figure 6A; $p < 0.01$; CAP versus control).

Since *VEGFA* mRNA expression was increased in response to CAP, we investigated if the corresponding

protein was also elevated. VEGFA binds with high affinity to VEGFR2 [31], whereas PDGFB interacts with PDGFR β [32]. Supernatants and cellular extracts from a confluent layer of HMVECs were collected 24 h after treatment with CAP. Samples were loaded on an SDS-PAGE gel and immunoblotted with anti-VEGFR2, anti-PDGFR β , and anti- β -tubulin antibodies (Figure 6B). The levels of VEGFR2 and PDGFR β in the total protein extracts were increased in response to CAP treatment (Figure 6B; $p < 0.05$; CAP versus control). Supernatants from HMVECs were analysed for secreted VEGF by ELISA. A significantly higher concentration of VEGF was detected in CAP-treated samples than in controls (Figure 6C; $p < 0.05$). To investigate if CAP was able to activate VEGFR signalling by inducing VEGFR2 phosphorylation, endothelial cells were treated with helium (control), CAP, or rhVEGF, and immunolabelled with anti-pVEGFR2 and anti-VEGFR2 antibodies (Figure 6D). Indeed, CAP, but not helium, induced phosphorylation of VEGFR2 (Figure 6D), suggesting that activation of VEGFR2 by phosphorylation is specific to CAP.

eNOS and its bioactive product NO are well-established pro-angiogenic molecules [10]. To determine if CAP activated eNOS signalling, protein extracts from CAP-treated HMVECs were immunoblotted with p-eNOS alongside equal protein levels of helium-treated controls (Figure 6E). Phosphorylation of eNOS was detected in HMVECs treated with rhVEGF (positive control), as well as in CAP-treated samples. Pretreatment of HMVECs with L-NAME (an inhibitor of NO synthase) led to a two-fold decrease in eNOS phosphorylation compared with the control (Figure 6E; $p < 0.05$; L-NAME versus control).

To determine if CAP is capable of rescuing the inhibitory effect of L-NAME, cells were firstly pretreated with L-NAME and then exposed to CAP. Indeed, CAP induced a four-fold increase in p-eNOS levels, suggesting that CAP restored eNOS phosphorylation blocked by L-NAME (Figure 6E; $p < 0.05$; L-NAME versus L-NAME + CAP). Taken together, these results suggest that CAP-modulated eNOS/NO signalling occurs via mechanisms illustrated in the supplementary material, Figure S4.

Discussion

Skin grafting is a technique particularly useful in burn wound reconstruction as well as surgical repair of chronic ulcers and defects resulting from tumour resection [33]. In reconstructed wounds, the skin graft is the scaffold system, which after successful integration is capable of producing the extracellular matrix. Angiogenesis is a crucial component of skin graft integration. Failure to establish a satisfactory blood supply between the donor graft and the recipient vascular wound bed leads to graft loss [5,32]. Our evidence suggested that the angiogenic effect of CAP was, at least

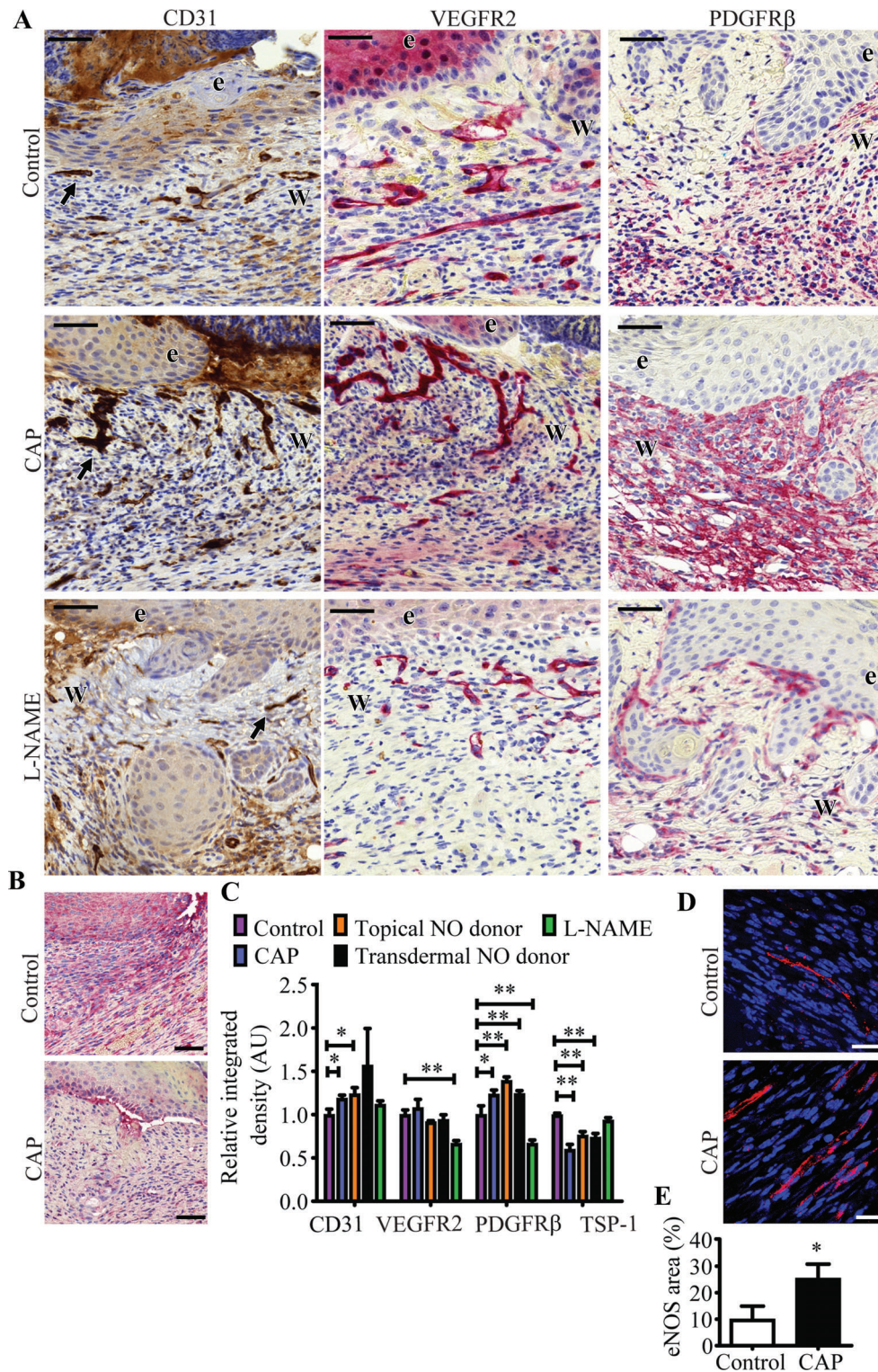


Figure 5. Enhanced angiogenesis in CAP-treated wounds was associated with increased expression of eNOS *in vivo*. (A) Representative immunohistochemistry images of day 7 mouse wounds stained for CD31, VEGFR2, and PDGFRβ. Note intense brown staining in CD31⁺ and red staining in VEGFR2⁺ blood vessels (indicated with arrows) in the dermis. In all images, e denotes the position of the epidermis and W indicates the position of the wound. Scale bar = 50 μm. Thrombospondins (TSPs) are a family of anti-angiogenic matricellular proteins. (B) Representative images of alkaline phosphatase-based immunohistochemistry of day 7 mouse wounds stained with anti-TSP-1 antibody. TSP-1 expression was decreased in CAP-treated burn wounds compared with helium controls. (C) Quantitative microdensitometric evaluation of day 7 wounds labelled with CD31 (endothelial cell marker), pro-angiogenic VEGFR2 and PDGFRβ, and anti-angiogenic TSP-1. Immunohistochemistry analysis was performed based on six fields of microscopic views of six independent wounds. Mean ± SEM (n = 6, *p < 0.05; **p < 0.01, Mann–Whitney U-test). (D) Assessment of eNOS expression *in vivo*. Immunofluorescence staining and representative images of eNOS (red) in day 7 mouse wounds were treated with either helium (control) or CAP. Nuclei were stained with DAPI (blue). (E) Quantitative evaluation of immunofluorescence detection of eNOS in day 7 mouse wounds. Immunofluorescence staining was performed in triplicates, and the data for statistical analyses were obtained from six fields of microscopic view of six independent wounds (n = 6; *p ≥ 0.05; Student's t-test).

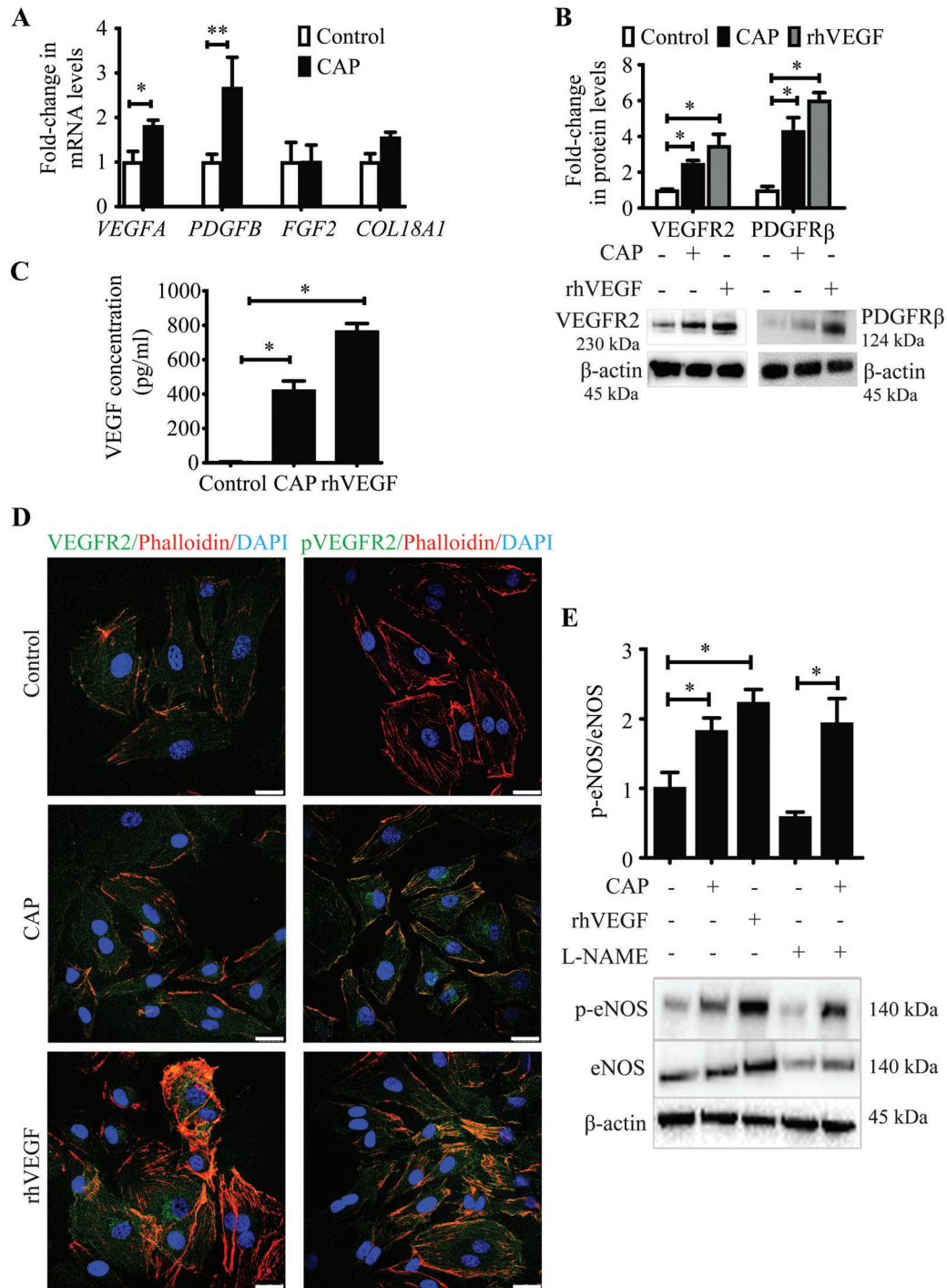


Figure 6. CAP treatment is associated with activation of VEGF and eNOS signalling *in vitro*. (A) To determine if CAP treatment is associated with differential expression of known activators and inhibitors of angiogenesis *in vitro*, RNA was isolated from either helium-treated (control) or CAP-treated monolayers of HMVECs. RT-qPCR analysis of pro-angiogenic *VEGFA*, *PDGFB*, *FGF2*, and anti-angiogenic *COL18A1* at 6 h after treatment with CAP. Mean \pm SEM ($n=6$, * $p < 0.05$; ** $p < 0.01$, Mann-Whitney *U*-test). (B) Representative western blots and bar graph showing the fold-change in the levels of VEGFR2 and PDGFR β in HMVECs treated with either helium (control), CAP, or rhVEGF (100 ng/ml; 5 min; positive control), calculated from three replicates of immunoblot data. Values are the means \pm SEM ($n=4$, * $p < 0.05$, Student's *t*-test). CAP treatment resulted in a significant increase of VEGFR2 and a concomitant increase in PDGFR β . (C) Cellular monolayers of HMVECs were treated with either helium (control), CAP, or hrVEGF (100 ng/ml; positive control). Twenty-four hours after the treatment, conditioned medium was collected and analysed using ELISA. The data analysis is expressed as the values for repeated conditions in separate wells ($n=3$, * $p < 0.05$, Student's *t*-test). (D) VEGF regulates angiogenesis by signalling through VEGFR2. To determine if CAP activates VEGFR2 through phosphorylation, HMVECs were treated with either helium (control), CAP, or rhVEGF (100 ng/ml; positive control, 5 min). Confocal immunofluorescent images of HMVECs immunostained for VEGFR2 (green) or pVEGFR2 (green). Filamentous actin was counterstained with phalloidin (red) and nucleus was stained with DAPI (blue). CAP induced phosphorylation of VEGFR2 ($n=3$). Scale bar = 20 μ m. (E) To determine if CAP activated eNOS, protein phosphorylation studies were performed. eNOS phosphorylation was assessed in HMVECs treated with CAP, rhVEGF (100 ng/ml; 5 min; positive control), or NO synthase (L-NAME; 100 μ M; 1 h; negative control). Protein extracts were immunoblotted for eNOS, p-eNOS, and β -actin. Bar graph shows p-eNOS/eNOS ratio. Values are the means \pm SEM of three replicates of immunoblot data ($n=3$, * $p < 0.05$, Student's *t*-test).

partly, due to enhanced cellular migration facilitated by CAP-generated RONS produced in plasma-activated media or transferred from the plasma gas phase to the aqueous media solution, where they dissolve, diffuse, and interact with cells [34]. Although the question of how CAP-generated RONS are delivered to cells remains unanswered, our data together with recent reports suggest that exposure to low doses of CAP promotes angiogenesis *in vitro* [35,36]. It is reasonable to assume that active molecules that diffuse from culture media into cells are also able to move across the skin. Accordingly, previous studies demonstrated that transdermal treatment with CAP altered the microcirculation as deep as 8 mm under the surface of the skin [21] and that higher doses of physical plasma induced solid tumour regression [34,37]. This suggests that the transfer of CAP-generated molecules through the skin is indeed possible. Having established that CAP promoted angiogenic responses *in vitro* and *in vivo*, we next investigated if NO is the chemical species that stimulated angiogenesis. NO was investigated as a candidate for several reasons. Firstly, NO is produced by plasma jets that operate in ambient air [18,34]; secondly, NO diffuses easily across cell membranes and penetrates skin [15,21]; thirdly, NO enhances angiogenesis [8,13]; and fourthly, NO is known to promote tissue [14,38] and burn wound [13] repair.

Having established that CAP enhanced endogenous NO synthesis, we next determined if CAP had the capacity to enhance burn wound closure. We hypothesised that a low dose of CAP would act as a platform for the delivery of therapeutic levels of biologically active species, including NO. Indeed, CAP increased the bioavailability of NO *in vitro* and improved burn wound healing *in vivo* through increased cellular proliferation and, possibly, other previously described NO-related mechanisms. This includes the enhancement of extracellular matrix formation and wound angiogenesis as demonstrated in second-degree burns [16], diabetic wounds [12], excisional wounds [38], and other dermatological lesions [14].

Given that NO is known to improve angiogenesis in tissue repair models [8] and that CAP is an efficient NO-generating platform [21], it is likely that the enhanced wound healing induced by the low doses of CAP is partly due to increased wound angiogenesis. Herein, we showed that CAP effectively increased the formation of microvessels both *in vivo* and *in vitro*. Our *in vivo* results showed that the levels of VEGF in CAP-treated burn wounds remained unchanged. A characteristic increase in VEGF levels may have occurred in the first few days after the injury. VEGF levels probably stabilised by day 7 as the wound entered the proliferative phase of healing. This is in accordance with several studies highlighting the importance of vessel maturation and timely return of VEGF to basal levels [31,39], warranting a fine balance between the expression of pro- and anti-angiogenic factors within the healing wound. Moreover, TSP-1, an anti-angiogenic factor with an important role in vessel regression and 'capillary pruning'

[40], was downregulated in the CAP-treated wounds. PDGF plays a vital role in the resolution and maturation phase of wound angiogenesis and is currently the only FDA-approved growth factor used for wound therapy [40]. Interestingly, our results showed that CAP treatment resulted in increased PDGFR β levels in the mouse wounds. Taken together, these findings provide a possible explanation for more durable and functional vessels within Matrigel plugs *in vivo*. The pro-angiogenic effect of CAP was supported by its stimulatory effect *in vitro* on VEGFA – a molecule known to enhance angiogenesis by signalling through VEGFR2 [32]. Here, we showed that CAP was able to modulate VEGF signalling either by modulating VEGFR2 concentration or by activating its signalling via phosphorylation.

It is likely that increased NO and VEGF levels in CAP-treated endothelial cells facilitated angiogenesis *in vitro* and *in vivo*. Future studies are required to explore whether angiogenic responses induced by CAP are either directly related to NO activity or are VEGF-dependent.

eNOS protein [encoded by the *nitric oxide synthase (NOS3)* gene] is transcriptionally regulated by growth factors including VEGFA [41]. Given that CAP stimulated the VEGF/VEGFR2 pathway, it was hypothesised that the endogenous NO synthase/NO pathway was also activated. Accordingly, CAP stimulated signal transduction causing eNOS phosphorylation, which accounted for increased endogenous NO production. Indeed, H₂O₂ generated by CAP is known to mediate eNOS transcription through oxidant-responsive kinases such as p38 mitogen-activated protein kinase [27]. This suggests that eNOS/NO signalling was probably activated by CAP-generated RONS. Indeed, eNOS expression increased in CAP-treated burn wounds, suggesting that CAP enhanced eNOS synthesis and, as a consequence, increased endogenous NO bioavailability.

In conclusion, this study indicates that CAP increases endogenous NO production, favouring the pro-angiogenic effect of NO *in vitro*, and results in improved wound neovascularisation *in vivo*. Further elucidation of the molecular mechanisms modulated by CAP will allow the development of novel therapeutic strategies that will improve a burn patient's quality of life.

Acknowledgements

This work was supported by L' Agence Innovation Défense de la Délégation Générale de L'Armement (DGA) and École Polytechnique. We thank Maryline Favier and Rachel Onifarasoaniaina of Institut Cochin for sample preparation and consultation. We also thank Dr Bruno Honnorat of École Polytechnique for his expertise and helpful advice.

Author contributions statement

NF, J-JL, and AR conceived and designed the experiments. CD carried out all experiments. NF and CD

acquired, analysed, and interpreted data. SB contributed substantially to analysis and interpretation of data. NF wrote the manuscript. All the authors contributed to manuscript preparation and approved the final submitted and published versions.

References

1. Peck MD. Epidemiology of burns throughout the world. Part I: distribution and risk factors. *Burns* 2011; **37**: 1087–1100.
2. Forbes SJ, Rosenthal N. Preparing the ground for tissue regeneration: from mechanism to therapy. *Nat Med* 2014; **20**: 857–869.
3. Finnerty CC, Jeschke MG, Branski LK, *et al.* Hypertrophic scarring: the greatest unmet challenge after burn injury. *Lancet* 2016; **388**: 1427–1436.
4. Sun BK, Siprashvili Z, Khavari PA. Advances in skin grafting and treatment of cutaneous wounds. *Science* 2014; **346**: 941–945.
5. Ramsey ML, Patel BC. *Full Thickness Skin Grafts*. StatPearls Publishing: Treasure Island, FL, 2018.
6. Eming SA, Wynn TA, Martin P. Inflammation and metabolism in tissue repair and regeneration. *Science* 2017; **356**: 1026–1030.
7. Schafer M, Werner S. Cancer as an overhealing wound: an old hypothesis revisited. *Nat Rev Mol Cell Biol* 2008; **9**: 628–638.
8. Kapila V, Sellke FW, Suuronen EJ, *et al.* Nitric oxide and the angiogenic response: can we improve the results of therapeutic angiogenesis? *Expert Opin Investig Drugs* 2005; **14**: 37–44.
9. Dulak J, Jozkowicz A, Dembinska-Kiec A, *et al.* Nitric oxide induces the synthesis of vascular endothelial growth factor by rat vascular smooth muscle cells. *Arterioscler Thromb Vasc Biol* 2000; **20**: 659–666.
10. Frank S, Kampfer H, Wetzler C, *et al.* Nitric oxide drives skin repair: novel functions of an established mediator. *Kidney Int* 2002; **61**: 882–888.
11. Yu J, deMuinck ED, Zhuang Z, *et al.* Endothelial nitric oxide synthase is critical for ischemic remodeling, mural cell recruitment, and blood flow reserve. *Proc Natl Acad Sci U S A* 2005; **102**: 10999–11004.
12. Edmonds ME, Bodansky HJ, Boulton AJ, *et al.* Multicenter, randomized controlled, observer-blinded study of a nitric oxide generating treatment in foot ulcers of patients with diabetes ProNOx1 study. *Wound Repair Regen* 2018; **26**: 228–237.
13. Nichols SP, Storm WL, Koh A, *et al.* Local delivery of nitric oxide: targeted delivery of therapeutics to bone and connective tissues. *Adv Drug Deliv Rev* 2012; **64**: 1177–1188.
14. Del Rosso JQ, Kircik LH. Spotlight on the use of nitric oxide in dermatology: what is it? What does it do? Can it become an important addition to the therapeutic armamentarium for skin disease? *J Drugs Dermatol* 2017; **16**: s4–s10.
15. Oplander C, Romer A, Paunel-Gorgulu A, *et al.* Dermal application of nitric oxide *in vivo*: kinetics, biological responses, and therapeutic potential in humans. *Clin Pharmacol Ther* 2012; **91**: 1074–1082.
16. Singer AJ, Choi Y, Rashel M, *et al.* The effects of topical nitric oxide on healing of partial thickness porcine burns. *Burns* 2018; **44**: 423–428.
17. Zhu H, Wei X, Bian K, *et al.* Effects of nitric oxide on skin burn wound healing. *J Burn Care Res* 2008; **29**: 804–814.
18. Gan L, Zhang S, Poorun D, *et al.* Medical applications of nonthermal atmospheric pressure plasma in dermatology. *J Dtsch Dermatol Ges* 2018; **16**: 7–13.
19. Heinlin J, Zimmermann JL, Zeman F, *et al.* Randomized placebo-controlled human pilot study of cold atmospheric argon plasma on skin graft donor sites. *Wound Repair Regen* 2013; **21**: 800–807.
20. Kaushik NK, Ghimire B, Li Y, *et al.* Biological and medical application of plasma-activated media, water and solutions. *Biol Chem* 2018; **400**: 39–62.
21. Isbary G, Morfill G, Schmidt HU, *et al.* A first prospective randomized controlled trial to decrease bacterial load using cold atmospheric argon plasma on chronic wounds in patients. *Br J Dermatol* 2010; **163**: 78–82.
22. Heuer K, Hoffmanns MA, Demir E, *et al.* The topical use of non-thermal dielectric barrier discharge (DBD): nitric oxide related effects on human skin. *Nitric Oxide* 2015; **44**: 52–60.
23. Ruzehaji N, Kopecki Z, Melville E, *et al.* Attenuation of flightless I improves wound healing and enhances angiogenesis in a murine model of type 1 diabetes. *Diabetologia* 2014; **57**: 402–412.
24. Ruffrok AC, Johnston DA. Quantification of histochemical staining by color deconvolution. *Anal Quant Cytol Histol* 2001; **23**: 291–299.
25. Liang CC, Park AY, Guan JL. *In vitro* scratch assay: a convenient and inexpensive method for analysis of cell migration *in vitro*. *Nat Protoc* 2007; **2**: 329–333.
26. Martinez LR, Han G, Chacko M, *et al.* Antimicrobial and healing efficacy of sustained release nitric oxide nanoparticles against *Staphylococcus aureus* skin infection. *J Invest Dermatol* 2009; **129**: 2463–2469.
27. Farah C, Michel LYM, Balligand JL. Nitric oxide signalling in cardiovascular health and disease. *Nat Rev Cardiol* 2018; **15**: 292–316.
28. Clough GF. Role of nitric oxide in the regulation of microvascular perfusion in human skin *in vivo*. *J Physiol* 1999; **516**(Pt 2): 549–557.
29. Seo HR, Jeong HE, Joo HJ, *et al.* Intrinsic FGF2 and FGF5 promotes angiogenesis of human aortic endothelial cells in 3D microfluidic angiogenesis system. *Sci Rep* 2016; **6**: 28832.
30. Kim J, Miranda AC, Popel AS, *et al.* Gene delivery nanoparticles to modulate angiogenesis. *Adv Drug Deliv Rev* 2017; **119**: 20–43.
31. Simons M, Gordon E, Claesson-Welsh L. Mechanisms and regulation of endothelial VEGF receptor signalling. *Nat Rev Mol Cell Biol* 2016; **17**: 611–625.
32. Carmeliet P, Jain RK. Molecular mechanisms and clinical applications of angiogenesis. *Nature* 2011; **473**: 298–307.
33. Valencia IC, Falabella AF, Eaglstein WH. Skin grafting. *Dermatol Clin* 2000; **18**: 521–532.
34. Yan D, Sherman JH, Keidar M. Cold atmospheric plasma, a novel promising anti-cancer treatment modality. *Oncotarget* 2017; **8**: 15977–15995.
35. Arndt S, Unger P, Berneburg M, *et al.* Cold atmospheric plasma (CAP) activates angiogenesis-related molecules in skin keratinocytes, fibroblasts and endothelial cells and improves wound angiogenesis in an autocrine and paracrine mode. *J Dermatol Sci* 2018; **89**: 181–190.
36. Miller V, Lin A, Kako F, *et al.* Microsecond-pulsed dielectric barrier discharge plasma stimulation of tissue macrophages for treatment of peripheral vascular disease. *Phys Plasmas* 2015; **22**: 122005.
37. Keidar M, Walk R, Shashurin A, *et al.* Cold plasma selectivity and the possibility of a paradigm shift in cancer therapy. *Br J Cancer* 2011; **105**: 1295–1301.
38. Shekhter AB, Serezhenkov VA, Rudenko TG, *et al.* Beneficial effect of gaseous nitric oxide on the healing of skin wounds. *Nitric Oxide* 2005; **12**: 210–219.
39. Lange C, Storkebaum E, de Almodovar CR, *et al.* Vascular endothelial growth factor: a neurovascular target in neurological diseases. *Nat Rev Neurol* 2016; **12**: 439–454.
40. Okonkwo UA, DiPietro LA. Diabetes and wound angiogenesis. *Int J Mol Sci* 2017; **18**: 1419.
41. Bogdan C. Nitric oxide and the immune response. *Nat Immunol* 2001; **2**: 907–916.

- *42. Baker M, Robinson SD, Lechertier T, *et al.* Use of the mouse aortic ring assay to study angiogenesis. *Nat Protoc* 2011; **7**: 89–104.
- *43. Ruzehaji N, Frantz C, Ponsoye M, *et al.* Pan PPAR agonist IVA337 is effective in prevention and treatment of experimental skin fibrosis. *Ann Rheum Dis* 2016; **75**: 2175–2183.
- *45. Schmittgen TD, Zakrajsek BA, Mills AG, *et al.* Quantitative reverse transcription-polymerase chain reaction to study mRNA decay: comparison of endpoint and real-time methods. *Anal Biochem* 2000; **285**: 194–204.
- *45. Lundberg JO, Weitzberg E, Gladwin MT. The nitrate–nitrite–nitric oxide pathway in physiology and therapeutics. *Nat Rev Drug Discov* 2008; **7**: 156–167.
- *Cited only in supplementary material.

SUPPLEMENTARY MATERIAL ONLINE

Supplementary materials and methods

Figure S1. Dose-dependent effect of CAP on endothelial cell viability

Figure S2. Cell migration is enhanced in response to CAP treatment

Figure S3. Cellular proliferation is increased in CAP-treated burns *in vivo*

Figure S4. Proposed overview of the mechanism of action of CAP-generated RONS and activation of eNOS/NO signalling in endothelial cells

50 Years ago in *The Journal of Pathology*...

Histology and prognosis in malignant melanoma

A. J. Cochran

Pulmonary fluid content in infants with respiratory distress

D. J. Desa

Pathology of recurrent oral ulceration and oral ulceration in behcet's syndrome: Light, electron and fluorescence microscopy

Thomas Lehner

Delayed hypersensitivity response in guinea-pig oral mucosa

D. Adams, J. J. Williamson, A. E. Dolby

To view these articles, and more, please visit:

www.thejournalofpathology.com

Click 'BROWSE' and select 'All issues', to read articles going right back to Volume 1, Issue 1 published in 1892.

The Journal of Pathology
Understanding Disease

